Electronic Supplementary Material (ESI) for Journal of Materials Chemistry C.

Electronic Supplementary Information

Solution-processed silver sulphide nanocrystal film for resistive switching memories

Beatriz Martín-García,† Davide Spirito,*† Roman Krahne and Iwan Moreels*

Istituto Italiano di Tecnologia. Via Morego 30, 16163 Genova (Italy)

$Ag_{2-x}S$ NC characterisation. *Transmission electron microscopy* (TEM) images were acquired with a 100 kV JEOL JEM-1011 microscope equipped with a thermionic gun. Samples were drop casted onto carbon-coated 200 mesh copper grids for the measurements. From the TEM measurements, an average NC diameter of *ca.* 3 nm was obtained (**Fig. S1a**).

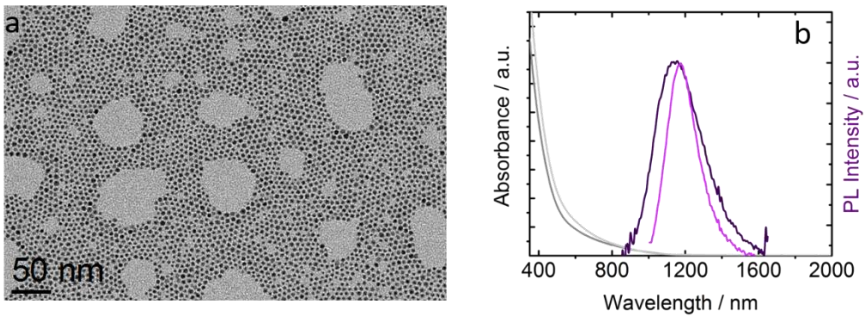

Fig. S1. (a) Representative TEM image of $Ag_{2-x}S$ NCs. (b) Absorbance and photoluminescence spectra of two $Ag_{2-x}S$ NC batches dispersed in TCE.

Absorption spectra were recorded with a Varian Cary 5000 UV-vis-NIR spectrophotometer. The *steady-state photoluminescence* (PL) emission was collected using an Edinburgh Instruments FLS920 spectrofluorometer, exciting the samples at 400 nm. The absorption spectrum does not show any distinct features. However, the synthesised NCs show a NIR PL emission around 1200 nm, which is in agreement with other $Ag_{2-x}S$ NCs reported in literature.[1,2] As shown in **Fig. S1b**, the PL emission properties are reproducible from batch to batch.

Elemental analysis was performed on digested NC solutions by inductively coupled plasma-optical emission spectrometry (ICP-OES). Samples were prepared in a 25 mL volumetric flask, drying a known amount of toluene solution under N_2 flow, and digesting the dry residue

overnight in two different acid media: (i) in 2.5 mL of aqua regia ($HCl:HNO_3$, 3:1vol) for standard analysis, and (ii) in HNO_3 for an improved Ag detection. Prior to the measurements, the samples were diluted to a total volume of 25 mL with Millipore water, and stirred with a vortex mixer for 10 s at 2400 rpm. Then, the sample was filtered using a PTFE membrane (0.45µm pore size, Sartorius®). Measurements were carried out with a ThermoFisher ICAP 6000 Duo inductively coupled plasma optical emission spectrometer. Three measurements were performed on each sample to obtain an averaged value, and three different synthesis batches were measured to yield an average Ag:S stoichiometry of (1.4 ± 0.1) : (1). Being substoichiometric, the $Ag_{2-x}S$ crystal favours memory effects by increasing the electron conductivity.[3]

X-Ray diffraction (XRD) analysis was performed with a PANanalytical Empyrean X-ray diffractometer equipped with a 1.8 kW CuKα ceramic X-ray tube, PIXcel^{3D} 2x2 area detector and operating at 45 kV and 40 mA. Samples for the XRD measurements were prepared in a glove box by drop casting a concentrated $Ag_{2-x}S$ NC dispersion onto a miscut silicon wafer. The diffraction patterns were collected using a Parallel-Beam (PB) geometry and symmetric reflection mode. According to the XRD data, the crystal structure of the colloidal $Ag_{2-x}S$ NCs corresponds to the acanthite (α-Ag_2S) phase together with some cubic metallic Ag inclusions (**Fig. S2a**). Note that, although the β-Ag_2S (argentite) phase presents superionic properties, it is only stable at temperatures higher than 177°C.[4,5] We have tried to obtain β-Ag_2S, however, neither synthesis at 250°C (**Fig. S2b**) nor annealing an α-Ag_2S film at 250°C (**Fig. S2c**) yielded the β-phase crystal structure (**Fig. S2d**). Likely, during the cooling process a relaxation of the crystal structure from argentite to acanthite occurs.

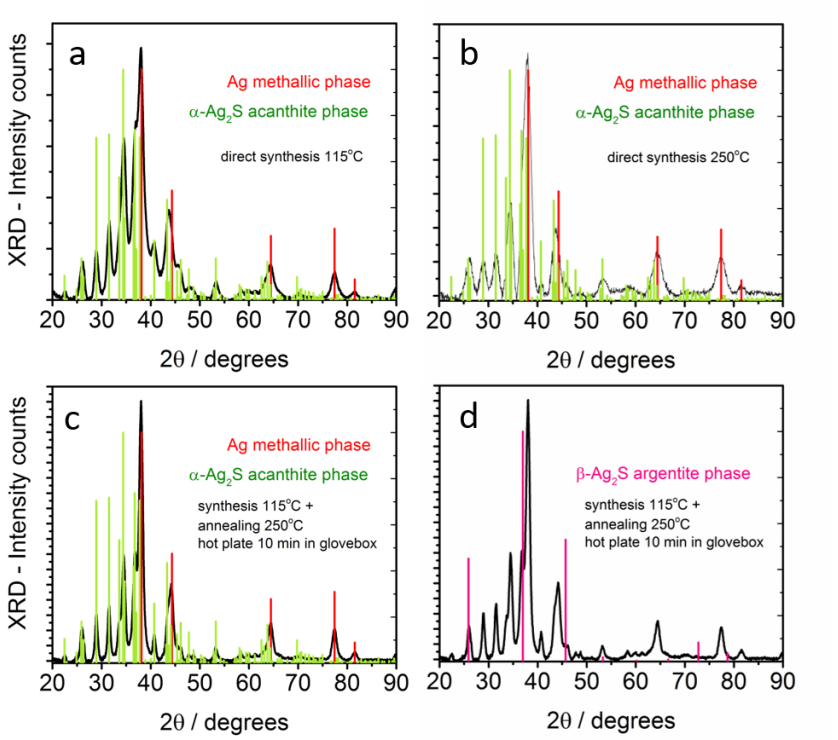

Fig. S2. XRD spectra of $Ag_{2-x}S$ NCs samples from direct synthesis at 115˚C (a) and 250˚C (b) together with the results from annealing at 250˚C in inert atmosphere of sample (a) (c, d). The XRD reference patterns of metallic silver (cubic, code 98-042-6921), acanthite Ag_2S (monoclinic, code 98-003-0445) and argentite Ag_2S (cubic, code 98-000-9586) are from the ICSD database and shown as vertical lines.

Additional optical and SEM images for Ag/$Ag_{2-x}S$/Ag macroscale system.

To complement the information of Fig. 1 in the main text, in **Fig. S3** we included detailed images collected with optical microscope and SEM, in which it is possible to observe the formation of the Ag metallic protrusions at the Ag negative electrode (noted as cathode for ECM devices[6]) and an Ag depletion at the anode (**Fig. S3b**). **Fig. S3c** also highlights how the Ag protrusions growth follows the direction of the electrical field.

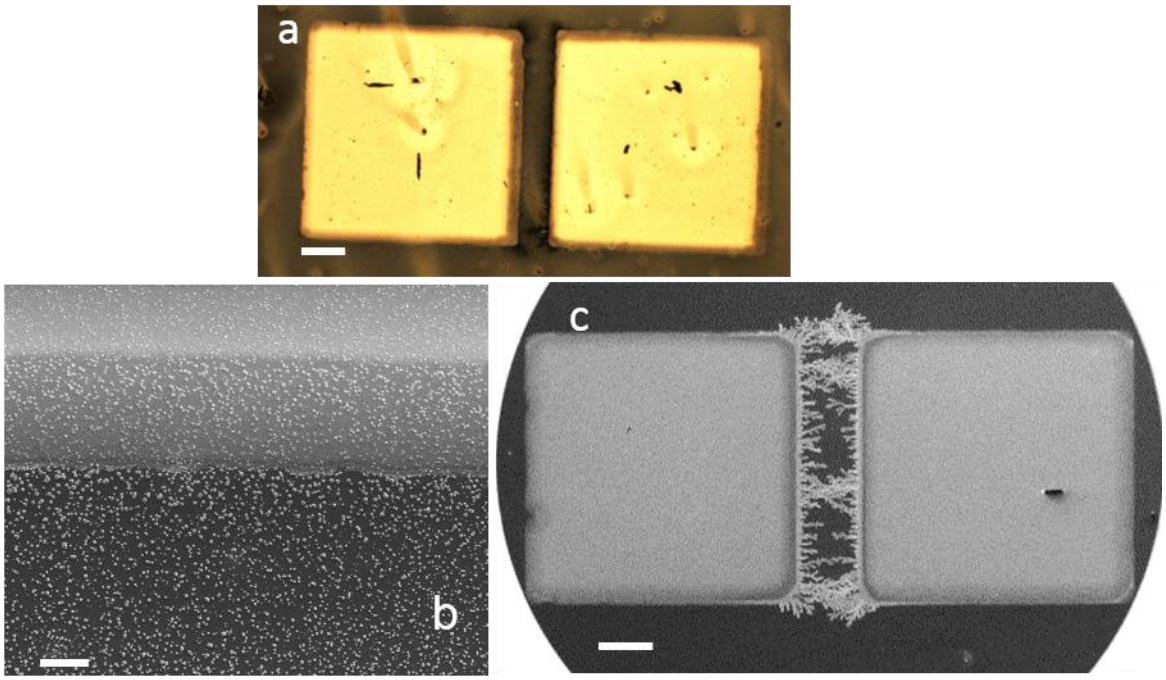

Fig. S3. (a) Optical image of a representative Ag/$Ag_{2-x}S$/Ag device. Scale bar is 200 µm. (b, c) SEM images of a representative Ag/$Ag_{2-x}S$/Ag device with film thickness of 20 nm, showing the area of the Ag contact where it is possible to observe the Ag depletion and the state of the device after several DC voltage sweeps. As shown in the SEM image in (c), dendrites are formed along the electric field lines. Scale bars are 10 (b) and 200 (c) µm, respectively.

SEM/EDX analysis of Ag/$Ag_{2-x}S$/Ag macroscale system.

Complementary SEM/EDX analysis is shown in **Fig. S4** for a representative Ag/$Ag_{2-x}S$/Ag macroscale device. The EDX mapping shows the accumulation of Ag in the protrusions, while the S signal remains constant along the film.

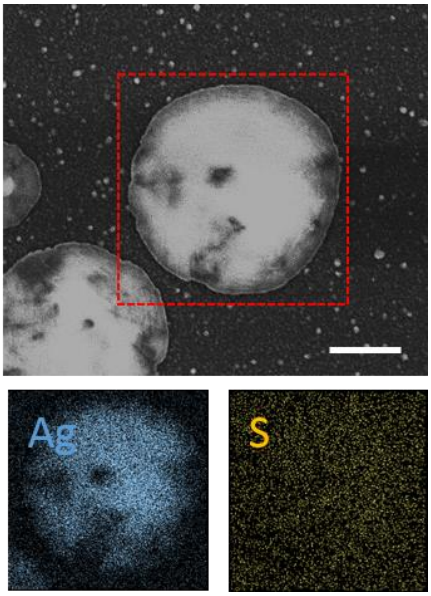

Fig. S4. SEM image of a single Ag protrusion. Red box marks the area analysed by EDX mapping. Scale bar is 500 nm. The lower panels show EDX maps acquired in the area marked in main panel for Ag (Lα1, 2.98 keV) and S (Kα1, 2.31 keV) lines, respectively.

Control experiments: vacuum and high voltage

Control experiments under vacuum demonstrated that protrusions with similar morphology to the ones in air are formed, **Fig. S5a-b,** indicating that the reaction is happening with the sulphur rather than the oxygen (or moisture) in air. Moreover, the IV characteristics collected under vacuum show the same features (within the variability we observed between different samples and devices) in comparison with the ones in air, indicating that no more species are involved in the switching mechanism, **Fig. S5c-d**. Additionally, the endurance is not improved in vacuum (**Fig. S5e**).

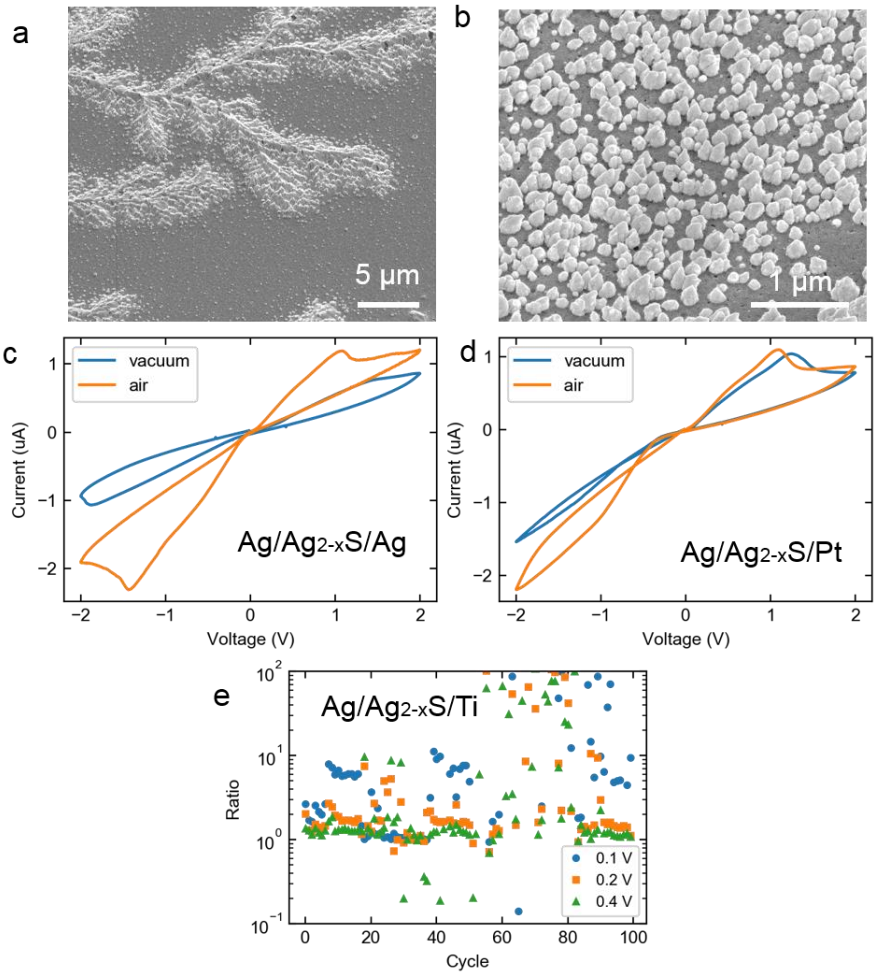

Fig. S5. Representative SEM images for Ag/$Ag_{2-x}S$/Ag (a) and Ag/$Ag_{2-x}S$/Pt (b) 'macroscale' devices after electrical measurements performed under vacuum. IV characteristics collected in vacuum and in air conditions for Ag/$Ag_{2-x}S$/Ag (c) and d) Ag/$Ag_{2-x}S$/Pt (d) 'macroscale' devices. The measurements in air are the same reported in the main text. (e) Multi-read' experiment in an Ag/$Ag_{2-x}S$/Ti 'macroscale' device in vacuum. All the experiments were performed as described in the main text of the paper, except for the use of a probe station under vacuum (pressure ~10^{-5} mbar) for the measurements.

We also measured cycles starting at 0V, up to 5V, down to -5 V and back to 0 V for representative Ti/$Ag_{2-x}S$/Ag analogous to Fig. 3a (main text) and Ag/$Ag_{2-x}S$/Ag devices, under air and vacuum conditions (**Fig. S6).** The trend for the first loop (positive) is very similar to cycles up to 2 V, but when the voltage becomes negative (approximately from -2V), the formation of a large metallic (Ag) dendritic structure contacts the two electrodes and results in a very high current (denoted by a sudden vertical line). The formation of the large dendritic structure is mostly irreversible since the filament remains and keeps short-circuiting the device.

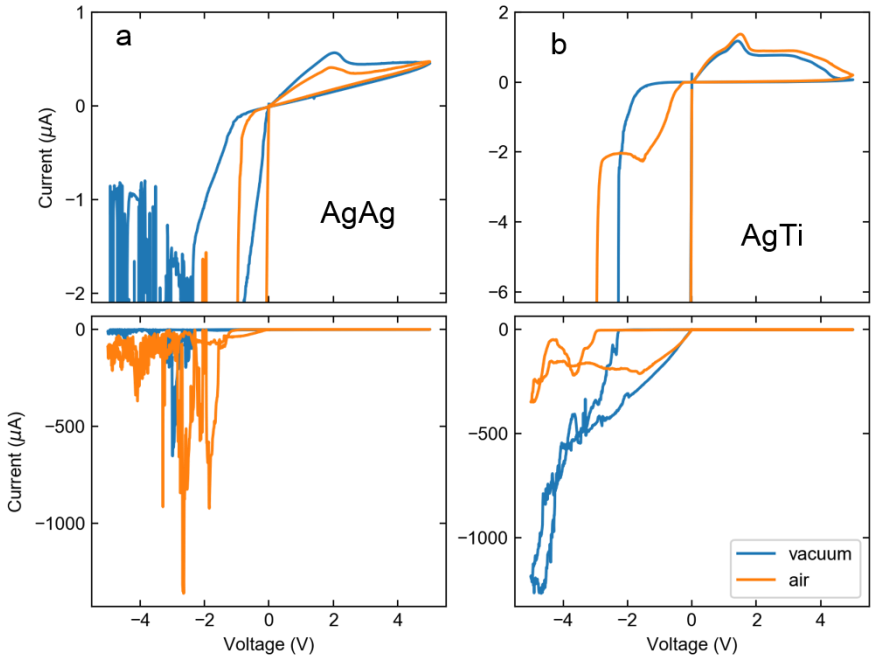

Fig. S6. Representative IV cycles up to 5V in 'macroscale' devices, collected in vacuum (blue) and in air (orange) conditions, for Ag/$Ag_{2-x}S$/Ag (a) and Ag/$Ag_{2-x}S$/Ti (b) systems. The lower panels show the upper curves at full scale.

Pre-activation protocols and switching tests.

As mentioned in the main text, to stabilize the first set/read/reset cycles reading, we established a pre-activation protocol. In **Fig. S7a**, we show a scheme of the procedure for the initial formation operation (0 → 2V) and the subsequent 'multi-read' protocol. **Fig. S7b-d** include pre-activated and non-pre-activated data in different devices, highlighting how the initiation of the ion migration across the $Ag_{2-x}S$ film by the initial voltage ramp reduces the number of cycles required to reach a stable measurement.

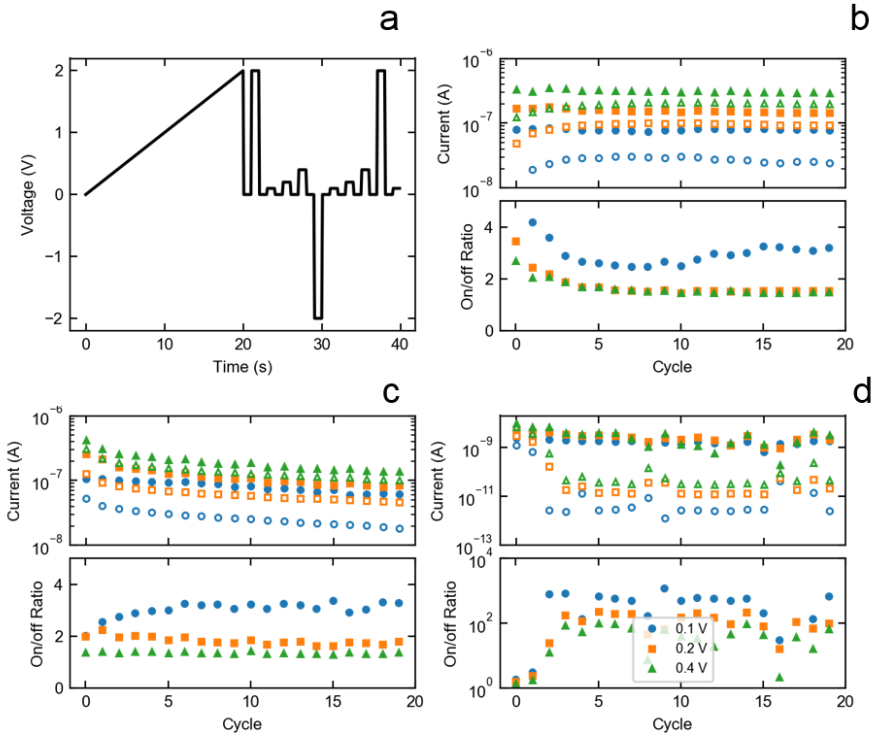

Fig. S7. (a) Pre-activation procedure (voltage as a function of time): after a linear ramp from 0 to 2 V, we start the set/read/reset cycles. (b-d) Effect of the activation on set/reset cycles. Upper panels: ON (full symbols) and OFF (empty symbols) current for set/reset cycles measured with V_{read}= 0.1 V (●), 0.2 V (■) and 0.4 V (▲). The I_{ON}/I_{OFF} ratio at the different read voltages is reported in the lower panels. (b) $Ag/Ag_{2-x}S/Ag$ macro-scale device, pre-activated with the procedure in panel (a). The ratio stabilizes to 3.0±0.1 after 4 cycles. (c) $Ag/Ag_{2-x}S/Ti$ macro-scale device, not pre-activated, reaches a stable ratio after 4 cycles (for a pre-activated device, see Fig. 3c in the main text). (d) Ti/Ag, tip/tip micro-scale device fabricated by EBL. The device was not pre-activated before the set/reset cycles, and shows a significant increase in I_{ON}/I_{OFF} ratio during the first 4 read cycles.

SEM/EDX analysis of Ti/$Ag_{2-x}S$/Ag macroscale system.

Complementary SEM/EDX analysis is shown in **Fig. S8** for a representative macroscale device with inert electrode: Ag/$Ag_{2-x}S$/Ti. The EDX maps demonstrate that no diffusion of Ti occurs during the device operation.

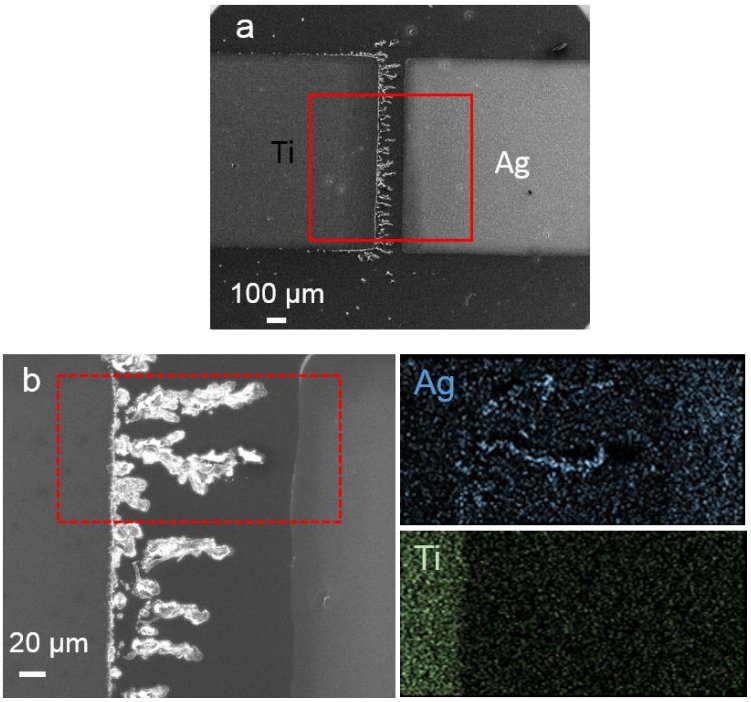

Fig. S8. (a, b) SEM images of a representative Ti/$Ag_{2-x}S$/Ag device with two different magnifications, showing the dendrite formation at the Ti electrode. The red box in (a) marks the area shown in **Fig. 3a** in the main text. EDX mapping analysis of the dendrites is included in (b). The dashed box marks the area analysed by EDX; the panels on the right show the intensity maps for Ag (Lα1, 2.98 keV) and Ti (Kα1, 4.51 keV) lines.

Switching tests on different electrode geometries prepared by EBL

Apart from the data shown in the main text, **Fig. 4**, focused on the tip-tip electrode geometry, here we include results for the other geometries explored (**Fig. S9**). A representative example for I_{ON}/I_{OFF} ratio, obtained by applying the 'multi-read protocol', for a flat-flat configuration in a Pt/$Ag_{2-x}S$/Ag device is shown in **Fig. S9a**, resulting in a best ratio of 115±28 (V_{read} = 0.2-0.4V), while results for a representative Ti/$Ag_{2-x}S$/Ag tip-flat device are shown in **Fig. S9b**, demonstrating a best ratio of 651±139 (V_{read} = 0.1V).

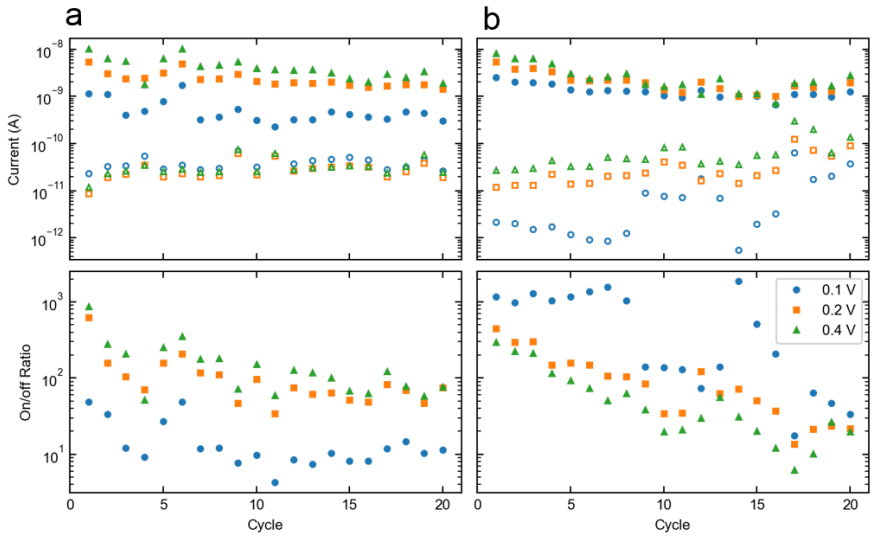

Fig. S9. Set/reset cycles measured with V_{read} = 0.1 V (●), 0.2 V (■) and 0.4 V (▲) for (a) flat(Pt)/flat(Ag) and (b) tip(Ti)/flat(Ag) devices with a 20 µm gap. I_{ON} (full symbols) and I_{OFF} (empty symbols) for both are displayed in the upper panels, and the I_{ON}/I_{OFF} ratio in lower panels. Ag was used as cathode (-); devices were pre-activated before measurements.

Focusing on the best tip-tip configuration, Ag/$Ag_{2-x}S$/Ti device, we performed set/read/reset test up to 100 cycles in different samples, **Fig. S10**, verifying that we obtained reproducible switching of the EBL fabricated devices only up to 20 cycles.

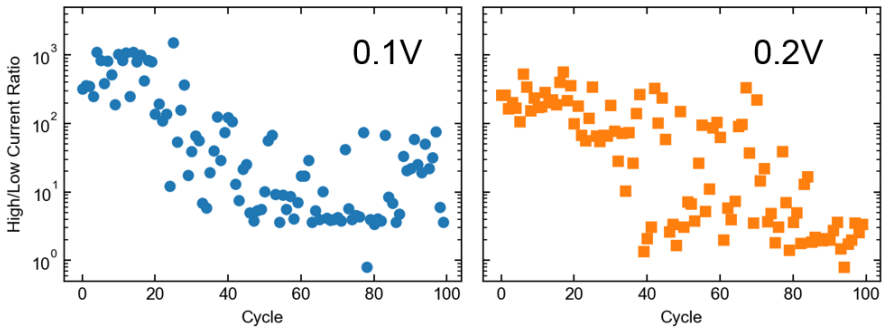

Fig. S10. Evolution of the I_{ON}/I_{OFF} ratio at V_{read} = 0.1 (right) and 0.2 V (left) for two different tip-tip Ag/$Ag_{2-x}S$/Ti devices stressed during 100 cycles of SET/RESET (±2 V) and read in air.

Supplementary Movies

The movies were acquired with a stereomicroscope (Olympus® SZX7) coupled to a CCD camera (Olympus® UC30). The original resolution of the video was 1040x772 pixels, acquired without compression; the files present in the supplementary were compressed, and finally overlays were added to assist the interpretation.

Movie 1

Movie 1 was acquired on an $Ag/Ag_{2-x}S/Ag$ macroscale device (pad 1x1 mm^2) during a voltage sweep from 0 V to +2 V, to -2 V and finally back to 0 V analogous to **Fig. 2a** in the main text. The bottom electrode is connected to ground (cathode (-)), while the voltage was applied to the top electrode (anode (+)). The voltage is shown in the video only for selected values during the linear sweep of the measurements. Red arrows mark the formation of dendrites and the depletion of Ag in the electrode.

Movie 2

Movie2 2 was acquired during pulse cycles with high voltage value of +5 V and -5 V of 1 s duration, to speed up the Ag dendrite growth, in an $Ag/Ag_{2-x}S/Ag$ macroscale device (pad 1x1 mm^2). The bottom electrode is connected to ground (cathode (-)), while the voltage was applied to the top electrode (anode (+)). In the video the labels "+" and "-" symbols identify where the positive and negative potential is applied at each step. It is possible to observe that the dendrites form from the negative electrode.

Supplementary references

(1) Doh, H.; Hwang, S.; Kim, S. Size-Tunable Synthesis of Nearly Monodisperse Ag_2S Nanoparticles and Size-Dependent Fate of the Crystal Structures upon Cation Exchange to $AgInS_2$ Nanoparticles. *Chem. Mater.* **2016**, *28* (22), 8123–8127.

(2) Lin, S.; Feng, Y.; Wen, X.; Zhang, P.; Woo, S.; Shrestha, S.; Conibeer, G.; Huang, S. Theoretical and Experimental Investigation of the Electronic Structure and Quantum Confinement of Wet-Chemistry Synthesized Ag_2S Nanocrystals. *J. Phys. Chem. C* **2015**, *119* (1), 867–872.

(3) Riess, I. Mixed Ionic–Electronic Conductors—Material Properties and Applications. *Solid State Ion.* **2003**, *157* (1–4), 1–17.

(4) Lutz, C.; Hasegawa, T.; Chikyow, T. Ag_2S Atomic Switch-Based 'Tug of War' for Decision Making. *Nanoscale* **2016**, *8* (29), 14031–14036.

(5) Sadovnikov, S. I.; Gusev, A. I.; Rempel, A. A. An in Situ High-Temperature Scanning Electron Microscopy Study of Acanthite–Argentite Phase Transformation in Nanocrystalline Silver Sulfide Powder. *Phys. Chem. Chem. Phys.* **2015**, *17* (32), 20495–20501.
(6) Kozicki, M. N.; Mitkova, M.; Valov, I. Electrochemical Metallization Memories. In *Resistive Switching*; Ielmini, D., Waser, R., Eds.; Wiley-VCH Verlag GmbH & Co. KGaA: Weinheim, Germany, 2016; pp 483–514.